THE ASTROPHYSICAL JOURNAL, 386:248–259, 1992 February 10

STAR FORMATION IN TAURUS. I. THE *IRAS* FAINT SOURCE SURVEY

C. A. BEICHMAN[1]
Institute for Advanced Study and Jet Propulsion Laboratory

F. BOULANGER
Ecole Normale Supérieure, 24 Rue Lhomond, Paris, 75005, France, and
Infrared Processing and Analysis Center, Jet Propulsion Laboratory

AND

M. MOSHIR[1]
Infrared Processing and Analysis Center, Jet Propulsion Laboratory
Received 1991 May 22; accepted 1991 August 2

ABSTRACT

A deep infrared survey of a 187 deg^2 region in Taurus using the *IRAS* Faint Source Survey reveals 63 multiband objects selected on the basis of their infrared properties. Two-thirds of the sample are previously uncataloged and are most likely either deeply embedded objects or unidentified T Tauri stars. Complete *IRAS* data are presented for these objects. The sample is estimated to be more than 90% complete for objects emitting $L \geq 0.1\ L_\odot$ between 12 and 60 μm. The luminosity function shows a decline at luminosities below $0.3\ L_\odot$. As noted by Kenyon et al., the shape of the luminosity function is difficult to understand in terms of standard models of protostellar accretion. The formation of a massive, $0.1\ M_\odot$, disk of circumstellar material serving as a reservoir for infalling cloud material represents a possible resolution of the problem. A population of unresolved sources emitting only at 60 μm is also identified. If any of these objects are self-luminous, they may represent the youngest protostellar objects yet observed.

Subject headings: infrared: stars — ISM: individual (Taurus Dark Cloud) — stars: pre–main-sequence — surveys

1. INTRODUCTION

Taurus is one of the premier regions for the study of the formation of solar-type stars. This paper presents a complete set of *IRAS* data for Taurus based on the *IRAS* Faint Source Survey, hereafter referred to as the FSS (Moshir et al. 1989). The FSS is approximately a magnitude more sensitive than the *IRAS* Point Source Catalog (Version 2, 1988, hereafter the PSC) at 12, 25, and 60 μm, but represents little or no improvement at 100 μm due to confusion by infrared cirrus (Low et al. 1984).

Two regions, Taurus and a control region on the opposite side of the Galactic plane from Taurus, were selected for study. This survey differs from the sample investigated by Beichman et al. (1986) and Myers et al. (1987), and the T Tauri star surveys of Strom et al. (1989) and Cohen, Emerson, & Beichman (1989), in that these studies were based on the presence of dense gas or young stars, as deduced from optical or millimeter-wave surveys. The present investigation presents an infrared selected sample, similar to, but more sensitive than that presented by Kenyon et al. (1990, hereafter KHSS). The FSS represents the most sensitive coaddition for point sources of *IRAS* data over large areas. Thus, the sample presented here will be the most complete, sensitive survey possible for some time in the mid- and far-infrared. An object emitting at the survey limits at 12, 25, and 60 μm would have a luminosity of $\sim 0.1\ L_\odot$ at the distance to Taurus, well below expected values for all but the earliest stages of the formation of stars of solar mass (Shu et al. 1987).

[1] Postal address: Caltech 100-22, Pasadena, CA 91125.

2. THE SAMPLE

2.1. *Sky Coverage*

Table 1 describes the sky coverage for this sample. The Taurus region is defined as a rectangular area in equatorial coordinates and is bounded by Perseus in the north and west and Orion in the east. The distance to this region varies from 350 pc in the northwest toward Perseus OB2 (Sargent 1979) to 160 pc for the bulk of Taurus (Elias 1978). Also defined is a control region that samples the same Galactic populations as Taurus except for those associated with star formation. Differences in the infrared populations of the two regions should be due mainly to the effects of young stars. The control region was obtained by reflecting the galactic latitudes, b, of the Taurus region about $b = 0°$. The control area lies in the northern part of the constellation Auriga. Table 1 also gives the extremes of the two regions in ecliptic and galactic coordinates which are useful in understanding certain aspects of the sample.

2.2. *Flux Criteria*

Sources in the FSS were drawn from Faint Source Data Base on the basis of criteria pertaining to signal-to-noise ratio (SNR) and confusion (Moshir et al. 1989). A basic selection criterion for the Faint Source Catalog (Moshir et al. 1989) was $b > 10°$ for 12 and 25 μm sources and $b > 20°$ for 60 μm. Since much of Taurus lies within 10–20° of the Galactic Plane, we could not use the Faint Source Catalog itself to find sources. Instead, all sources in this paper were drawn in a uniform manner from the Faint Source Data Base with the primary criterion that a source have at least one high quality measurement at either 12, 25, or 60 μm. A high quality measurement (BMFQUAL = 3) implies a signal-to-noise ratio (SNR) greater than 5. About two-thirds of the sources selected from the Faint

TABLE 1

TAURUS AND AURIGA REGIONS SURVEYED

Parameter	Taurus	Auriga
α(1950)	3^h50^m–5^h	5^h51^m–7^h
δ(1950)	21°–33°	36°–51°
min, max l^{II}	161°3–181°2	161°6–181°3
min, max b^{II}	−24°8–−5°2	5°2–22°6
min, max λ	59°4–77°3	88°2–102°4
min, max β	−1°7–12°6	12°6–28°1
Area (deg^2)	187	187

TABLE 2

DISTRIBUTION OF DETECTED WAVELENGTHS

IRAS DETECTION AT (μm)				TAURUS		AURIGA	
12	25	60	100	All	Final Sample	All	Final Sample
Y				663	(369)	583	(148)
	Y			2	(2)	3	(1)
Y	Y			221	9	273	3
		Y		178	(161)	241	(206)
Y		Y		15	0	6	0
	Y	Y		18	13	14	11
Y	Y	Y		105	18	63	2
			Y	11	(10)	9	(8)
Y			Y	4	0	4	0
	Y		Y	0	0	0	0
Y	Y		Y	1	0	0	0
		Y	Y	56	0	115	1
Y		Y	Y	3	0	3	0
	Y	Y	Y	6	5	19	11
Y	Y	Y	Y	41	18	26	1
Totals				1322	63	1359	29

NOTE.—Values in parentheses indicate the numbers of single-band sources without stellar or extragalactic associations. These objects do not meet the color criteria and are not included in the sample. Their numbers are listed here for reference.

Source Data Base were also in the Faint Source Catalog and are designated with an "F" in front of their names; the remainder of the sources were found only in the Faint Source Data Base and are denoted with a "Z" in front of their names.

IRAS made a minimum of three and as many as five hours-confirming scans of this part of Taurus (*IRAS* Explanatory Supplement 1988), and the number of observations per pixel in the co-added FSS plates ranges from 15 to more than 25. Studies at high galactic latitude (Moshir et al. 1989, p II-60ff) suggest that this combination of SNR and coverage means that the reliability of even the faintest sources exceeds 90% at 12 μm, 85% at 25 μm, and 75% at 60 μm. Since cirrus confusion makes it difficult to assess reliability at 100 μm, sources were not allowed into the sample only on the basis of a 100 μm detection. In this context, reliability is taken to mean that a celestial source exists at the stated position on the sky; whether that source is a piece of some more extended emission, i.e., cirrus, is a separate question that will be addressed below.

Maps of the noise in the co-added *IRAS* data show minimum values of 50, 50, and 60 mJy at 12, 25, and 60 μm in regions that received three or more hours-confirming scans with *IRAS*. Figures 1*a*–1*d* show the flux density in mJy at which the completeness is estimated to be 90% due to the effects of both detector noise and confusion. This completeness level was derived from the distribution of flux densities on the scale of ~ 1 deg^{-2}. The 87% quantile of the distribution was used to compute the width of a Gaussian distribution from which the 90% completeness level was estimated (Moshir et al. 1989). Variations of up to a factor of 2 in the floor of the survey are apparent across Taurus. In the interest of defining the deepest possible sample, all sources with at least one high quality measurement were initially considered as part of the sample. Once a source satisfied the criterion of at least one BMFQUAL = 3 detection, measurements in other bands were included if they had BMFQUAL of 2 or 3.

Despite the proximity of the regions surveyed to the Galactic plane (Table 1), the galactic longitudes are close to the anti-center and point source confusion is not a serious problem at 12 and 25 μm. The surface density of 12 μm detections in Taurus is 5.6 deg^{-2}, less than the confusion limit of 21 sources (deg^{-2}) required by demanding 75 beams per source. Confusion due to diffuse extended emission is, however, a serious problem at 60 and 100 μm and, as suggested by Figures 1*c* and 1*d*, limits the long-wavelength sensitivity of this survey in a highly nonuniform manner.

2.3. *Source Selection Criteria*

Both Taurus and the reference region contain over 1300 objects that meet the basic flux quality criteria described above (Table 2, column marked "All"). However, few of these sources are likely to be associated with star formation. Three techniques were used to eliminate irrelevant objects. First, objects associated with galaxies were rejected using the associations listed in the FSS. Second, the colors of the sources were used to eliminate field stars or stars associated with mass loss by demanding that the spectral energy distributions of sources be redder than both a Rayleigh-Jeans spectrum or the spectrum of mass-losing giant stars.

Figures 2*a* and 2*b* show the 12–25 and 25–60 μm colors of all objects in the Taurus and Auriga samples. A population of objects with normal stellar colors is seen in both regions, and is cleanly separated from a second, cooler population that exists predominantly in Taurus. As pointed out by Harris-Law, Clegg, & Hughes (1988) and Emerson (1989) there is a fairly clean separation between mass losing giants and objects associated with star formation such as T Tauri stars (Cohen et al. 1989) or embedded sources (Beichman et al. 1986). Color criteria at 12, 25, and 60 μm (Table 3) were designed by reference to Figure 2 and to observations of mass-loss stars (Zuckerman & Dyck 1986; Beichman et al. 1990). Examination of Figures 1 and 2 of Zuckerman & Dyck (1986) suggests that the 12–25 μm criterion will eliminate about three-quarters of the giant stars and that the 25–60 μm criterion will remove 95% of the giants detected in those bands. The color temperatures corresponding to these limits exclude sources hotter than 385 K at 12 and 25 μm, and 230 K at 25 and 60 μm. Neither the Taurus sample nor the Zuckerman & Dyck (1986) data were corrected for the broad passbands of the *IRAS* filters when these comparisons were made. Table 3 shows that even the hottest, optically selected T Tauri stars (Cohen et al. 1989) will not be discriminated against by these color criteria. Examination of color-color diagrams of normal galaxies (Helou 1986) suggest that these criteria *do not* filter out an appreciable fraction of galaxies.

Finally, a 60 and 100 μm color criterion was imposed to eliminate cold cirrus. As a further filter against cirrus and

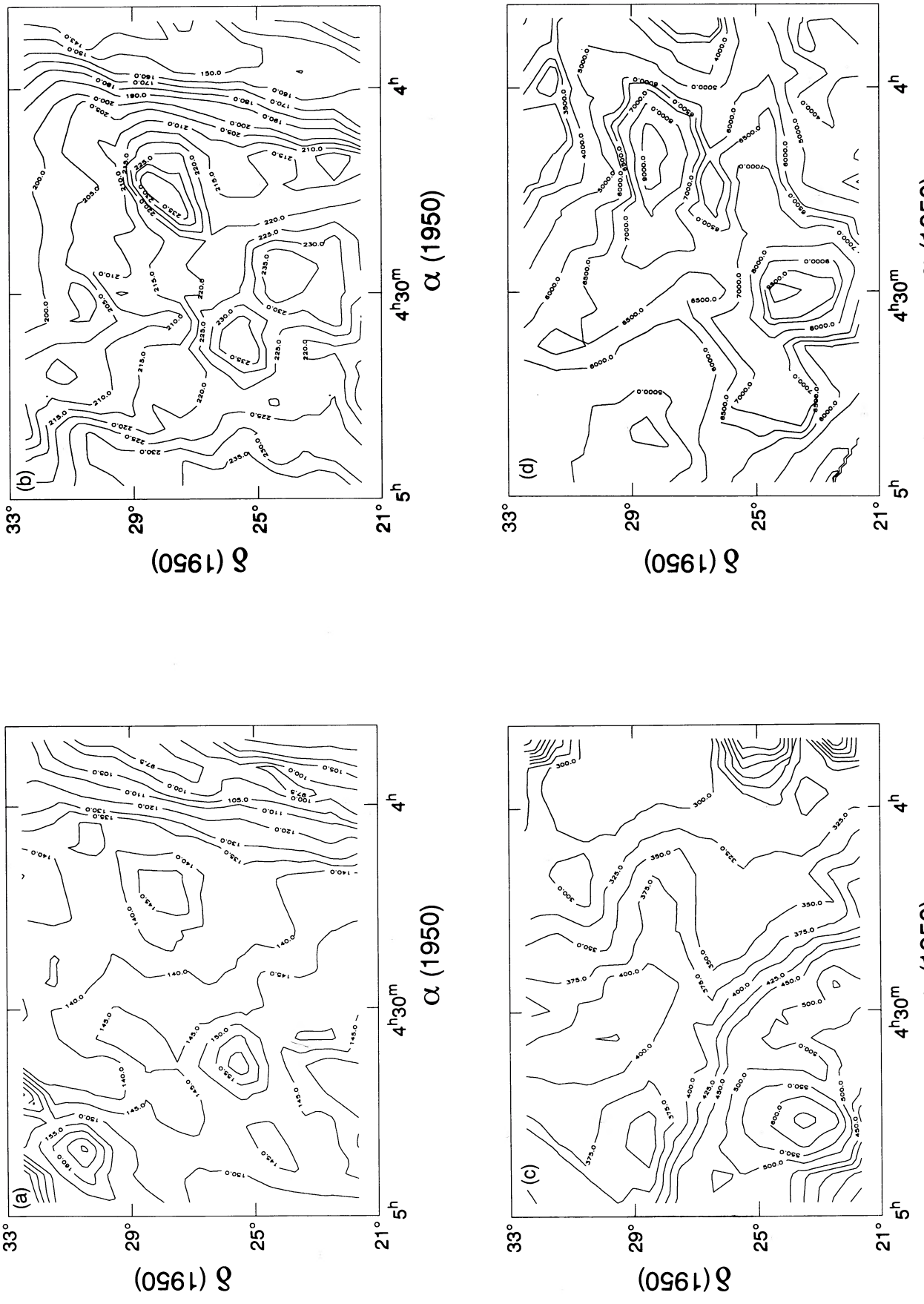

FIG. 1.—(*a–d*) Noise levels at 12, 25, 60, and 100 μm in mJy for which the estimated completeness is 90% or greater. The values are derived from a combination of detector noise and source density as described by Moshir et al. (1989).

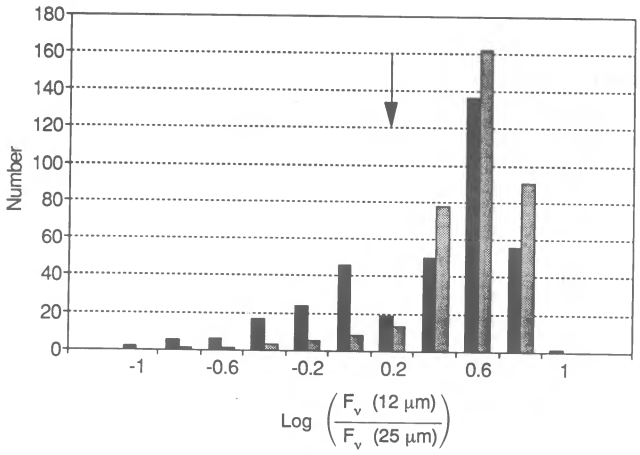

FIG. 2a

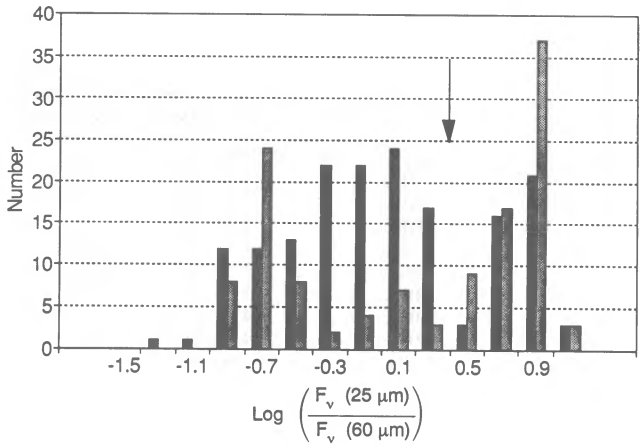

FIG. 2b

FIG. 2.—(*a*) Histogram of 12–25 μm color for Taurus (*dark shading*) and Auriga (*light shading*) regions shows an excess in Taurus of objects with a relatively flat 12–25 μm color. The arrow denotes the 12–25 μm criterion used for discriminating against stars. (*b*) The same as Fig. 2*a* except the 25–60 μm color is shown.

extended sources, sources detected solely at 60 and 100 μm had to have BMFQUAL = 3 at 100 μm. Only those sources satisfying all the color criteria appropriate to the detected wavelength bands were included in the final sample.

Of the 118 objects that met the color criteria of Table 3, 52 are associated with visible stars as determined from associations in the FSS, in the Catalog of Emission Line Stars (Herbig & Bell 1988), or in the SIMBAD data base. Of these, 40 are T Tauri stars tabulated in Cohen et al. (1989). The reminder are mostly early-type (~B7–A3) stars with strong infrared excesses. The data for these stars are not presented herein. An additional three sources, 04139+2737, 04214+3112, and 04356+3159, were excluded from the sample because their appearance on the Palomar Observatory Sky Survey (POSS) prints, their lack of CO emission (J. Bally 1990, private communication) or 1–3 μm colors (KHSS) strongly suggested that they are galaxies. Table 4 lists the remaining 63 sources in Taurus with energy distributions characteristic of young stellar objects and that are without previously studied stellar (or extragalactic) counterparts. As noted in Table 4, the FSS occasionally missed a detection at one or more wavelengths that could be filled in with reference to the PSC or addscans of specific objects (Beichman et al. 1986; KHSS). The flux densities in Table 4 *have been* color-corrected using flux density ratios in adjacent bands and the appropriate table from the *IRAS* Explanatory Supplement (1988). For the colors of the sources considered here the maximum corrections are ~20% at 12 and 25 μm, ~15% at 60 μm, and ~5% at 100 μm.

TABLE 3

SPECTRAL CRITERIA

Ratio	Adopted Value	Bluest Young Stars[a]	Remaining Fraction of Red Giants[b]
$\frac{F_\nu(12\ \mu m)}{F_\nu(25\ \mu m)}$	<1.2 (385 K)	0.7	0.25
$\frac{F_\nu(25\ \mu m)}{F_\nu(60\ \mu m)}$	<2 (230 K)	1.2	0.05
$\frac{F_\nu(60\ \mu m)}{F_\nu(100\ \mu m)}$	>0.1 and <3.2	0.8	

[a] Mean flux ratio plus $3\sigma_{mean}$ from Table 2 of Cohen et al. 1989.
[b] Zuckerman & Dyck 1986.

Derived properties for the sources are presented in Table 5. These include the luminosity, L_{IRAS}, derived according to the prescription of Emerson (1988) which uses the four *IRAS* passbands to derive a luminosity that extends, in the case of a four band source, from 7 to 135 μm. Submillimeter observations of a number of embedded sources (Beichman 1990; Ladd et al. 1991) suggest that the peak in the spectra of these objects occurs between 100 and 200 μm and that a simple extrapolation suffices to account for the radiation emitted at wavelengths longer than 100 μm. The table includes L_{inf} which is obtained by extrapolating the spectrum from the long-wavelength cutoff of longest detected wavelength band to infinite wavelength. The extrapolation is derived by fitting a blackbody curve to the two longest *IRAS* wavelengths with positive detections. The exact extrapolation technique is relatively unimportant as L_{inf} is usually a small correction to L_{IRAS}, averaging 14% and having a maximum value of 47%. The total far-infrared luminosity, L_{FIR}, is the sum of L_{IRAS} and L_{inf}.

Tables 5 and 6 present an assessment of the optical appearance of the object from examination of the POSS prints. The tables also give the results of searching the *IRAS* positional error ellipse for stellar candidates in the *HST* Guide Star Catalog (hereafter GSC; Lasker et al. 1989; Jenkner et al. 1989). In Taurus, the scan angles for the multiple scans were all roughly parallel, and inclined by less than 10° to the celestial equator, so that it is adequate to approximate the 2 σ error ellipse by a 60″ × 15″ rectangle with its long axis oriented east-west. Based on Monte Carlo simulations where random 60″ × 15″ position ellipses were compared with the GSC, more than 80% of these matches are likely to be real. Roughly 40% of the sample, those with optical ID classes 1–3 and 5, have a match in the GSC. The average separation between the FSS and GSC positions is 16″.

Finally, Table 5 presents $I_\nu(100\ \mu m)$ derived from a median-filtered 100 μm map of the region which gives an indication of amount of interstellar gas in the vicinity of each source. The

TABLE 4

TAURUS FAINT SOURCE SURVEY SAMPLE

Number	R.A. (1950)	Decl. (1950)	$F_\nu(12)$[a]	$F_\nu(25)$	$F_\nu(60)$	$F_\nu(100)$	References
01	$3^h50^m30^s.4$	32°29′59″	−0.09	0.16	0.71	−4.2	
02	3 51 47.8	29 50 55	0.28	0.23	−0.21	−2.8	
03	3 51 55.6	31 23 14	0.33	0.68	0.63	−3.1	
04	3 53 19.9	26 06 14	0.08	0.15	0.41	−3.1	
05	3 57 49.4	31 34 45	0.32	1.52	1.71	1.5[b]	c
06	3 58 09.1	28 27 16	−0.05	0.14	0.60	−3.7	
07	3 58 57.4	31 43 30	−0.08	0.23	0.71	2.4	
08	4 01 40.4	26 10 47	4.33	16.7	46.1	56.0	d, e
09	4 02 51.6	29 48 32	0.32	1.70	3.36	4.2	c
10	4 03 49.8	25 33 33	0.20	0.20	0.27	−4.2	
11	4 10 07.9	24 50 08	−0.98	0.23	0.78	−4.7	
12	4 10 50.4	29 10 46	0.39	0.48	0.35	−5.3	
13	4 10 52.6	28 04 05	1.3[b]	3.88	7.52	11.9	c
14	4 11 21.1	27 58 14	2.80	6.39	13.3	14.6	c
15	4 12 41.4	28 11 30	−0.14	0.20	0.37	−14.0	
16	4 14 42.4	28 22 16	0.25	0.24	−0.30	−3.4	
17	4 15 25.0	28 23 56	0.49	1.07	1.79	−4.5	
18	4 15 52.2	28 05 09	0.27	0.70	0.85	−8.7	c
19	4 16 36.1	27 08 52	−0.07	0.28	0.94	−25.7	
20	4 16 36.3	27 06 23	0.08[b]	0.67	5.38	11.0	c
21	4 16 53.4	27 02 46	0.80	5.56	16.0	17.6	c
22	4 17 17.6	27 56 53	−0.18	0.40	0.26	−4.1	
23	4 17 20.4	28 12 19	0.14	0.21	−0.20	−9.3	
24	4 19 12.3	26 47 52	0.29	0.30	−0.37	−10.4	
25	4 19 40.9	26 38 49	0.29	0.38	0.29	−3.3	
26	4 19 42.6	30 36 25	0.17	0.15	−0.29	−2.0	
27	4 20 02.2	27 59 04	0.33	0.49	0.60	−7.6	
28	4 21 39.3	26 03 21	0.33	0.45	0.93	−4.6	
29	4 23 53.4	24 36 52	2.02	7.14	15.2	17.1	
30	4 24 52.5	26 12 38	0.23	1.37	4.40	10.2	d, e
31	4 26 00.0	26 42 32	−0.10	0.33	0.99	−8.0	
32	4 26 18.0	26 54 57	0.27	0.56	0.36	−3.8	
33	4 26 28.0	24 33 23	0.51	3.12	5.13	−12.5	c
34	4 27 22.3	28 00 42	−0.21	0.34	0.40	−2.7	
35	4 27 51.8	22 53 45	11.1	11.7	7.63	7.4	c
36	4 29 33.2	22 51 08	0.71	1.75	3.57	8.6	
37	4 29 41.2	29 23 41	1.47	6.66	40.2	45.0	
38	4 29 47.5	22 46 42	0.78	0.92	0.54[b]	−14.2	c
39	4 29 54.7	27 14 55	0.14[b]	0.51	2.93	2.41[b]	c
40	4 30 09.4	26 08 07	−0.17	0.45	0.46	−5.4	
41	4 30 16.8	22 47 04	−0.09	0.51	6.23	9.3	c
42	4 30 19.1	22 40 18	2.30	2.56	1.38	−14.7	d, e
43	4 30 40.9	29 09 19	−0.11	0.17	0.47	−3.7	
44	4 30 49.8	26 07 09	0.29	0.38	0.29	−2.7	
45	4 32 34.3	24 02 13	−0.06	2.65	13.0	23.0	
46	4 36 03.8	23 31 52	−0.07	0.33	0.35	−2.1	
47	4 36 09.8	25 47 28	2.07	21.1	42.6	33.1	
48	4 36 14.3	31 00 47	−0.11	0.22	1.54	−4.3	
49	4 36 17.2	25 39 10	0.57	0.60	−0.49	−25.2	
50	4 36 31.2	25 35 54	1.38	9.75	36.0	38[f]	d, e
51	4 36 48.6	25 57 17	−0.09	0.82	18.7	71	
52	4 36 51.3	25 39 12	5.58	6.36	7.11	18[f]	c, d
53	4 37 05.1	25 59 41	0.41	0.54	−2.46	−56.1	
54	4 38 09.4	25 40 53	0.48	2.80	10.2	12.6	d, e
55	4 38 34.7	25 50 46	0.67	1.57	2.64	−5.8	d, e
56	4 41 04.1	28 07 35	0.12	0.24	0.94	4.2	
57	4 41 41.2	30 01 43	−0.08	0.18	0.58	−7.6	
58	4 45 03.8	29 19 39	0.30	0.29	−0.21	−1.8	
59	4 48 58.1	30 32 49	0.12	0.34	0.40	−2.8	
60	4 56 48.9	27 01 34	0.22	0.51	0.94	−3.6	c
61	4 57 00.1	25 20 29	0.27	0.20	−0.25	−2.9	
62	4 59 55.8	30 50 24	−0.08	0.19	0.42	4.2	
63	4 59 57.0	22 55 38	0.38	0.92	1.15	−1.5	c

[a] Flux densities (Jy) are color-corrected. Negative values denote 3 σ upper limits.
[b] Flux density from KHSS.
[c] Object also found in KHSS.
[d] Beichman et al. 1986.
[e] Myers et al. 1987.
[f] Flux density from Beichman et al. 1986.

TABLE 5

VISIBLE AND DERIVED PROPERTIES OF SAMPLE

Number	*IRAS* Name	Distribution (pc)	Optical ID Class[a]	V (mag)	$I_\nu(100\,\mu m)$ (MJy sr^{-1})	L_{IRAS} ($L_\odot$)	L_{inf} ($L_\odot$)	L_{FIR} ($L_\odot$)
1.....	Z03505+3229	350	2	15.3	2.4	0.16	0.050	0.21
2.....	F03517+2950	350	2	13.3	3.6	0.29	0.036	0.32
3.....	F03519+3123	350	1	11.5	2.7	0.53	0.036	0.57
4.....	F03533+2606	350	6		2.2	0.17	0.026	0.19
5.....	F03578+3134	350	1	11.6	0.5	1.02	0.040	1.06
6.....	Z03581+2827	350	3		2.1	0.13	0.042	0.17
7.....	Z03589+3143	350	3		1.7	0.34	0.152	0.49
8.....	F04016+2610	160	4		16.6	3.89	0.376	4.27
9.....	F04028+2948	160	1	12.4	4.9	0.31	0.029	0.34
10.....	F04038+2533	160	2	11.3[b]	2.4	0.05	0.003	0.06
11.....	Z04101+2450	160	3		6.1	0.04	0.011	0.05
12.....	F04108+2910	160	3	14.7[c]	5.4	0.10	0.004	0.11
13.....	F04108+2804	160	4		16.5	0.83	0.092	0.92
14.....	F04113+2758	160	4		13.8	1.43	0.092	1.52
15.....	Z04126+2811	160	4		14.6	0.02	0.005	0.03
16.....	F04147+2822	160	1	14.9	18.7	0.05	0.008	0.06
17.....	F04154+2823	160	4		19.0	0.20	0.022	0.22
18.....	F04158+2805	160	3		17.9	0.11	0.010	0.12
19.....	Z04166+2708	160	4		14.0	0.05	0.014	0.06
20.....	F04166+2706	160	4		16.6	0.38	0.100	0.48
21.....	F04168+2702	160	4		15.4	1.21	0.111	1.32
22.....	F04173+2756	160	1	14.1	8.0	0.03	0.003	0.04
23.....	Z04173+2812	160	3		9.1	0.03	0.008	0.04
24.....	F04192+2647	160	3		9.4	0.06	0.011	0.07
25.....	F04196+2638	160	3		7.4	0.08	0.003	0.08
26.....	F04197+3036	160	1	11.1	4.1	0.04	0.005	0.04
27.....	F04200+2759	160	3		10.7	0.10	0.007	0.11
28.....	F04216+2603	160	3		10.0	0.11	0.012	0.12
29.....	F04238+2436	160	6		15.2	1.45	0.109	1.56
30.....	F04248+2612	160	7		11.0	0.40	0.095	0.49
31.....	Z04260+2642	160	7		15.4	0.05	0.014	0.07
32.....	F04263+2654	160	7		15.4	0.09	0.004	0.09
33.....	F04264+2433	160	7		16.3	0.43	0.064	0.50
34.....	F04273+2800	160	3		10.4	0.03	0.005	0.04
35.....	F04278+2253	160	5	14.6	15.4	2.82	0.043	2.86
36.....	F04295+2251	160	7		17.0	0.44	0.083	0.52
37.....	F04296+2923	160	5	15.6[c]	25.3	2.56	0.291	2.85
38.....	F04297+2246	160	1	14.5[c]	15.9	0.20	0.006	0.20
39.....	F04299+2714	160	3		14.0	0.18	0.014	0.20
40.....	Z04301+2608	160	4		18.1	0.04	0.005	0.05
41.....	F04302+2247	160	4		17.7	0.36	0.072	0.43
42.....	F04303+2240	160	2[d]		17.6	0.57	0.015	0.58
43.....	Z04306+2909	160	6		11.6	0.03	0.006	0.03
44.....	F04308+2607	160	1	13.6	19.2	0.08	0.003	0.08
45.....	F04325+2402	160	4		26.1	0.89	0.192	1.08
46.....	Z04360+2331	160	3		11.0	0.03	0.004	0.04
47.....	F04361+2547	160	4		31.4	3.45	0.186	3.64
48.....	Z04362+3100	160	3		3.8	0.06	0.025	0.09
49.....	F04362+2539	160	1[d]		30.3	0.13	0.021	0.15
50.....	F04365+2535	160	4		35.0	2.47	0.239	2.71
51.....	F04368+2557	160	4		35.0	1.64	1.269	2.91
52.....	F04368+2539	160	7		34.8	1.74	0.190	1.93
53.....	F04370+2559	160	4		23.7	0.09	0.019	0.11
54.....	F04381+2540	160	4		27.2	0.74	0.086	0.83
55.....	F04385+2550	160	1		20.6	0.28	0.033	0.32
56.....	Z04410+2807	160	5[e]		9.3	0.12	0.074	0.19
57.....	Z04416+3001	160	4		5.5	0.03	0.008	0.04
58.....	Z04450+2919	160	3		3.0	0.07	0.010	0.08
59.....	Z04489+3032	160	3		4.9	0.05	0.005	0.06
60.....	Z04568+2701	160	6		12.7	0.10	0.012	0.11
61.....	F04570+2520	160	2	13.8	8.2	0.06	0.007	0.06
62.....	Z04599+3050	160	6		...	0.08	0.074	0.16
63.....	F04599+2255	160	2		...	0.50	0.014	0.16
			Average[f].....		14	0.58	0.074	0.65
			σ_{pop}.....		9	0.91	0.16	1.0

[a] Optical ID classes: (1) Obvious stellar counterpart; (2) Probable counterpart; (3) Multiple faint candidates; (4) Blank field; (5) Obvious nebulosity; (6) Faint stars with possible nebulosity; (7) Blank field with faint nebulosity.

[b] Second, 14 mag GSC candidate exists 10″ further away.

[c] GSC classifies as nonstellar.

[d] Object is a T Tauri star according to S. Kenyon 1990, private communication.

[e] Object is a galaxy according to S. Kenyon 1990, private communication.

[f] As described in the text, the statistics for the luminosity include the four sources missed in this sample, but found by other authors.

TABLE 6

SUMMARY OF OPTICAL PROPERTIES OF TAURUS SAMPLE

ID Class	POSS Description	Number in Sample	Number in GSC	Avg $I_\nu(100)$ (MJy sr^{-1})	*IRAS* Source Characteristics[a]
1.....	Obvious stellar candidate	10	8	12 ± 3	12 and 25, (60) μm
2.....	Probable candidate	6	4	7 ± 3	12 and 25 μm
3.....	Multiple faint candidates	16	1	8 ± 1	(12), 25, and 60 μm
4.....	Blank field	17	0	20 ± 2	4 band
5.....	Obvious nebulosity	3	11	16 ± 6	4 band
6.....	Faint stars with faint nebulosity	5	0	10 ± 3	(12), 25, and 60, (100) μm
7.....	Blank field with faint nebulosity	6	0	18 ± 4	4 band or 12, 25, 60 μm

[a] Wavelength bands typically detected by *IRAS*. Parentheses denote a band seen only in roughly half the sources.

7×7 point ($7' \times 7'$) median filter removes the effect of the source itself from the determination. Values range from 3 to 16 MJy sr^{-1}. The conversion from $I_\nu(100\ \mu m)$ to an estimate of the visual extinction depends on the intensity of the interstellar radiation field and the opacity of the region (Boulanger & Pérault 1988). For the diffuse interstellar medium in the solar neighborhood, the average ratio, $I_\nu(100\ \mu m)/A_V$, is 16 MJy sr^{-1} mag^{-1}. In dark clouds, the attenuation of the interstellar radiation field lowers this ratio significantly. For the Helies 2 cloud in Taurus and B5 in Perseus, $I_\nu(100\ \mu m)/A_V \sim 5$ MJy sr^{-1} mag^{-1}. The 100 μm brightness saturates at about 20 MJy sr^{-1}, a value above which $I_\nu(100\ \mu m)$ provides only a lower limit on A_V of about 4 mag (Cernicharo & Guélin 1987; Langer et al. 1989; Snell, Heyer, & Schloerb 1989). The values in Table 5 suggest that the average extinction in the vicinity of these sources ranges from less than 0.2 mag up to more than 4 mag.

2.4. *Single Band Sources*

Some of the sources detected only at a single *IRAS* wavelength are potentially of interest. For example, sources detected only at 12 μm might represent a population of luminous brown dwarfs or young stars with previously undiscovered disks. Objects detected only at 60 μm could be extremely cold objects deeply embedded in a molecular cloud that escaped detection at 100 μm due to cirrus confusion. On the other hand, sources detected only at 25 μm are few in number and are probably spurious at the low ecliptic latitudes considered here where asteroids and detector anomalies due to the high zodiacal background are troublesome. Finally, the vast majority of sources detected only at 100 μm are certainly cirrus condensations.

Taurus has about 13% more 12 μm only sources than the comparison region, with most of the excess coming at the lowest flux densities, ≤ 0.3 Jy, where completeness effects dominate the counts (Table 2). When known stars are removed from the two samples, the imbalance between the two regions increases with 369 unidentified 12 μm sources in Taurus compared with only 148 in Auriga. The large number of unidentified 12 μm sources in Taurus is consistent with the greater visual extinction in Taurus compared with Auriga. Even half a magnitude difference in the visual extinction through the two lines of sight could reduce the number of visibly cataloged background stars by a factor of 2 since stars of equal intrinsic brightness would fall below optical catalog limits in Taurus. The extended 100 μm emission detected by *IRAS* (Fig. 3, Plate 00) has a median surface brightness of 6 MJy sr^{-1} corresponding to $A_V \sim 1.5$ mag. Some areas having extinctions greater than this (Herbig 1977; Scalo 1990). Further, at least 0.5 mag of differential extinction between the two regions is implied by the $E(B-V)$ maps of Burstein & Heiles (1977). The large number of 12 μm only sources precludes their inclusion in this paper, but the list, including GSC matches, is available in electronic form from the authors.[2]

Sources without associations and detected only at 60 μm could be embedded sources, condensations or ridges in cirrus clouds, or galaxies whose visible and 100 μm counterparts have been obscured by cirrus. The FSS lists two parameters, FRATIO and CC (correlation coefficient) which help discriminate against cirrus. FRATIO can be thought of as the ratio of the flux densities of a source measured in two apertures, one appropriate to extended sources and one to point sources. Values of FRATIO larger than 1 denote sources with significant spatial extent in either the in-scan or cross-scan direction. CC measures the correlation between the measured source profile with a computed two-dimensional point source template. Since the Taurus region lies close to the ecliptic plane, the point source template remains simple after co-addition and CC should be effective at detecting small extensions in the scan direction.

A sample of 60 μm only objects was generated by taking sources with $F_\nu(60\ \mu m) > 0.5$ Jy at which the survey is thought to be close to 90% complete (Fig. 1*c*). Since Beichman et al. (1986) have shown that young stellar objects with luminosities less than a few $L_\odot$ should not be able to heat their surroundings enough to appear extended at the *IRAS* resolution, a self-luminous object emitting only at 60 μm should be unresolved. Figure 4 shows the distribution of CC and FRATIO for all objects in the Taurus region with a 60 μm detection. The concentration of sources likely to be galaxies (detections at 25 and 60 μm), or compact embedded objects (detections at 12, 25, 60, and 100 μm) around FRATIO ~ 1.0 and CC > 0.9 suggests that sources with this range of CC and FRATIO are likely to be compact, possibly self-luminous. On the other hand, sources likely to be cirrus (extended objects with 60 and 100 μm detections) have FRATIO > 1.2. Thirty-four sources were selected with $0.8 <$ FRATIO < 1.2 and CC > 0.9. Examination of the POSS prints shows that six of the 34 objects are galaxies. The 28 pointlike sources without obvious galaxy counterparts are listed in Table 7 along with an assessment of the POSS image and $I_\nu(100\ \mu m)$ as a measure of the amount of interstellar material. The flux density limits for the 60 μm only objects at 12 and 25 μm vary by less than a factor of 2 and are always less than 0.2 Jy at 12 μm and less than 0.25 Jy at 25 μm. The 100 μm limits vary considerably and are given in the table. Only three of these sources are in the Faint Source Catalog; the remainder lie below the $b = 20°$ cutoff for the catalog or were rejected for various confusion problems. The criteria on

[2] Contact C. Beichman at chas@ipac.Caltech.edu.

PLATE 6

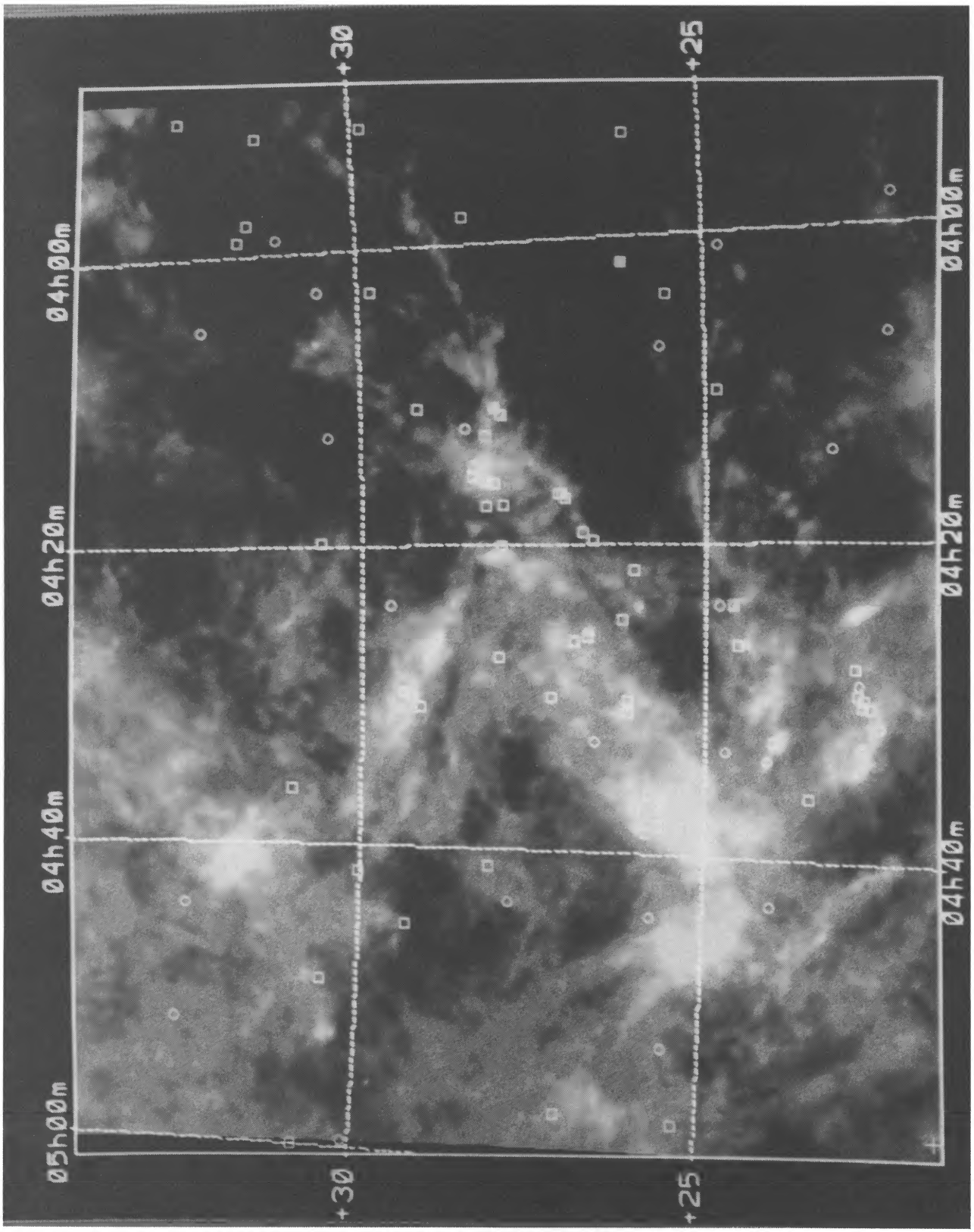

FIG. 3.—A 100 μm map of a 15° × 15° region in Taurus with the locations of the multiband and 60 μm only sources from Tables 4 and 7 marked as squares or circles, respectively.

BEICHMAN, BOULANGER, & MOSHIR (see 386, 254)

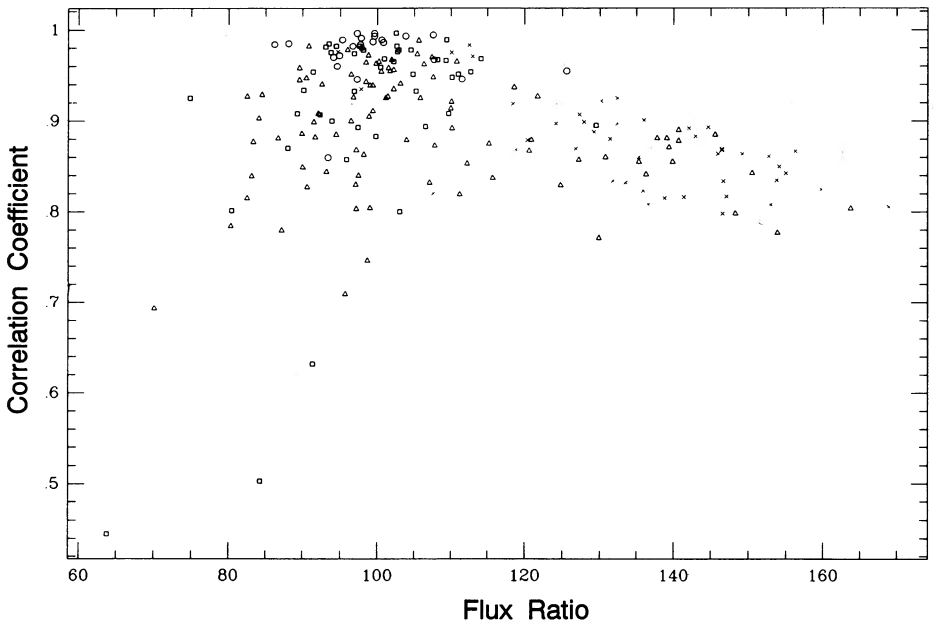

FIG. 4.—FRATIO vs. CC figure with different types of sources denoted with different symbols: 60 μm only objects as triangles; 25, 60 μm as squares; 60 and 100 μm objects as crosses; and four-band sources as circles.

TABLE 7

UNRESOLVED TAURUS 60 μm ONLY SOURCES

Number	R.A. (1950)	Decl. (1950)	$F_\nu(60)$[a] (Jy)	FRATIO	CC	$F_\nu(100)$ (Jy)	Distance (pc)	Optical ID[b]	$I_\nu(100\ \mu m)$ (MJy sr^{-1})	$L(30–75)$ ($L_\odot$)
64[c]	$3^h58^m02^s.6$	22°17′55″	0.58	0.93	0.94	−2.8	160	3	4.4	0.021
65	3 58 58.4	31 09 58	0.55	1.07	0.97	−2.7	350	6	1.1	0.094
66[c]	4 00 52.5	24 46 35	0.63	1.11	0.96	−5.5	160	6	6.6	0.023
67	4 02 19.3	21 14 21	0.92	0.96	0.98	−4.5	160	2	7.1	0.033
68	4 02 43.2	30 35 17	0.81	0.90	0.96	−4.8	160	2	4.7	0.029
69	4 05 02.6	32 18 47	0.53	1.12	0.93	−2.9	160	[d]	3.2	0.019
70	4 06 42.0	22 22 58	0.60	0.90	0.95	−6.9	160	3	6.9	0.022
71	4 07 11.8	25 39 11	0.58	1.00	0.96	−5.3	160	4	6.3	0.021
72[c]	4 12 09.6	28 29 31	0.79	1.14	0.97	−6.1	160	4	8.6	0.029
73	4 12 35.1	30 29 27	0.94	0.99	0.94	−1.9	160	3	1.0	0.034
74	4 14 02.4	23 12 27	0.55	1.03	0.93	−2.5	160	2	7.2	0.020
75	4 23 54.2	29 35 50	1.65	1.06	0.99	−6.1	160	3, jet	6.0	0.059
76	4 23 54.4	24 49 34	0.86	0.90	0.95	−6.4	160	2, jet	9.3	0.031
77	4 24 31.5	27 50 22	0.76	1.02	0.96	−8.9	160	6	11.6	0.027
78	4 28 52.3	22 50 55	0.66	1.01	0.93	−7.4	160	4	13.8	0.024
79	4 31 30.5	22 32 25	0.64	0.96	0.95	−8.6	160	4	20.7	0.023
80	4 32 50.4	26 35 52	0.85	1.10	0.91	−7.2	160	4	11.8	0.031
81	4 33 17.6	24 42 58	1.36	0.91	0.98	−6.9	160	4	12.4	0.049
82	4 33 47.3	24 07 05	0.72	1.19	0.93	−2.7	160	2	18.7	0.026
83	4 41 26.5	31 03 29	0.88	0.98	0.94	−3.4	160	4	6.9	0.032
84	4 42 52.1	24 03 18	0.69	0.99	0.91	−3.6	160	4	9.6	0.025
85	4 43 24.1	27 49 00	0.90	1.20	0.96	−3.7	160	3	7.5	0.032
86	4 43 59.3	25 45 15	0.52	1.02	0.97	−4.7	160	4	12.7	0.019
87	4 44 08.9	32 31 56	0.55	0.84	0.93	−2.0	160	3	4.9	0.020
88	4 51 41.3	24 08 49	0.61	1.01	0.94	−4.7	160	4	9.3	0.022
89	4 51 52.4	32 37 46	0.51	1.02	0.93	−4.5	160	6	3.0	0.018
90	4 52 13.0	25 31 23	1.20	1.00	0.96	−7.4	160	4[e]	9.6	0.043
91	4 59 30.7	30 06 57	0.64	0.82	0.93	−3.0	160	6	...	0.023
							Average		8.3	0.030
							σ_{pop}		4.0	0.015

[a] Flux densities (Jy) are *not* color-corrected. Negative values denote 3 σ upper limits.
[b] Optical ID Classes as described in Table 5.
[c] Source in Faint Source Catalog.
[d] Bright SAO star obscures field.
[e] Object is galaxy according to S. Kenyon 1990, private communication.

CC and FRATIO were designed to select the objects most likely to be self-luminous in a cirrus-full region.

2.5. *Survey Completeness*

The completeness levels of the survey vary with wavelength and position. At 12 and 25 μm the analysis of high-latitude sky (Moshir et al. 1989, pp. III-41ff) should be applicable to the present survey. At these wavelengths, the 90% completeness level for 13–25 counts per pixel should be $\sim$100 mJy. These values are within a factor of 2 of those given in the completeness maps (Figs. 1*a* and 1*b*) and vary in a way that is consistent with the coverage variations across the region. We estimate conservatively that the entire Taurus sample is 90% or more complete for sources brighter than 200 mJy at 12 and 250 mJy 25 μm. At longer wavelengths, cirrus makes the high-latitude analysis inapplicable, but the completeness maps (Figs. 1*c* and 1*d*) and examination of the FSS source counts suggest that the completeness in Taurus is 90% or greater at 0.6 Jy at 60 and at 10 Jy at 100 μm. Thus, except for the case of confusion due to nearby bright sources, we estimate that this survey is 90% complete for sources emitting at the survey limits at 12, 25, and 60 μm and having $L_{IRAS} \sim 0.1\ L_{\odot}$.

A measure of the effectiveness of the FSS source extractor at bright flux levels, an important component in the completeness of the survey, can be obtained by comparing PSC samples of the same area generated by other authors. All of the 12 objects found by Beichman et al. (1986) that should have appeared in the FSS samples (four with, and eight without stellar counterparts) were found. Similarly, comparing our sample with KHSS, the FSS sample contains 19 of a possible 22 objects. Of the 48 T Tauri stars found in the PSC and tabulated in Cohen et al. (1989), 42 appeared in the FSS sample with detections in at least one band. The object TMR-1 (Terebey et al. 1990) should have been in the FSS sample, but was not. Thus, the FSS sample missed 10 objects out of a possible 83, corresponding to 88% completeness at $\geq$1 Jy for 12, 25, and 60 μm. The missing 10% of the sample at these relatively bright flux density levels may be attributed to a relatively constant effect of confusion due to multiple or extended sources. The median filter used in generating the FSS is known to suppress sources under such conditions (Moshir et al. 1989, IIIa).

Sources that were missed in this sample but which meet all criteria for inclusion include the following: 03580+3135, 04181+2655, 04181+2654 (KHSS), and TMR-1 (Terebey et al. 1990; KHSS). These four sources are included in the various statistical discussions presented below.

We have also compared our results with the sources found in the *IRAS* Serendipitous Survey Catalog (Kleinmann et al. 1986) which used sensitive scans over limited areas to go deeper than the Point Source Survey. Estimates of the 3 σ noise within the individual $\sim$1 deg^2 fields in Taurus are 0.14, 0.33, 0.33, and 5.3 Jy at 12, 25, 60, and 100 μm, respectively. Estimates of the 90% completeness limits based on analysis of the log (N)–log (S) plots in each band give comparable values: 0.25, 0.28, 0.22, and 3 Jy. Given the factor of two uncertainties in the effects of confusion noise in the *IRAS* Serendipitous Survey, these values are quite similar to the completeness limits quoted in this paper.

3. DISCUSSION

3.1. *Nature of the Multiband Sources*

Although comparable numbers of multiband sources are seen in Taurus and the reference region, they differ in type between the two areas. A total of 36 sources are detected in Taurus in either all four bands, or at 12, 25, and 60 μm (Table 2). Since confusion can eliminate 100 μm detections easily, it is likely that many of the 12, 25, and 60 μm objects are similar to those detected in all four bands. Only three such sources were detected in Auriga. These three and four band sources are predominantly found in regions of high $I_{\nu}(100\ \mu\text{m})$ with no optical counterparts or in fields with nebulosity [Optical ID classes 4, 5, 7; and 6 with high $I_{\nu}(100\ \mu\text{m})$]. Both Taurus and Auriga show comparable numbers of objects detected at 25 and 60 μm or at 25, 60, and 100 μm in the two regions (18 for Taurus and 22 for Auriga). These objects are usually associated with faint optical candidates [ID classes 2, 3; and 6 with low $I_{\nu}(100\ \mu\text{m})$] and relatively low amounts of extinction. Many of these sources could be faint galaxies with high infrared to optical luminosity ratios.

The spatial distribution of the sources generally follows that of the interstellar material emitting at 100 μm, or seen in CO (Ungerechts & Thaddeus 1987) or NH_3 (Benson & Myers 1989). However, the occurrence of sources is far from uniform with several obvious groups of sources. The most prominent asterism consists of sources 47, 49, 50–55 and is located around $\alpha = 4^{h}37^{m}$ and $\delta = 26°$. This cluster is located within a ring of rotating gas in Helies Cloud 2 near TMC-1C (Schloerb & Snell 1984). The concentration of infrared sources in TMC1-C was first noted by Terebey et al. (1990). Other prominent groupings include sources 16, 17, 18, 22, and 23 in L1454; and a cluster (35, 36, 38, 41, 42) in L1536.

Although near-infrared photometry is not yet available for this sample, embedded sources with Optical ID classes 4, 6 and 7 are most likely Class I objects in the classification scheme of Adams, Lada, & Shu (1987). Class I objects have spectral energy distributions that rise steeply into the infrared with more than 90% of the luminosity of these sources emitted in the *IRAS* bands (Myers et al. 1987; KHSS). The luminosity function for sources with optical classes of 4–7 is shown in Figure 5 and can be compared directly with Figure 8 of KHSS. The data presented here extend the luminosity function a

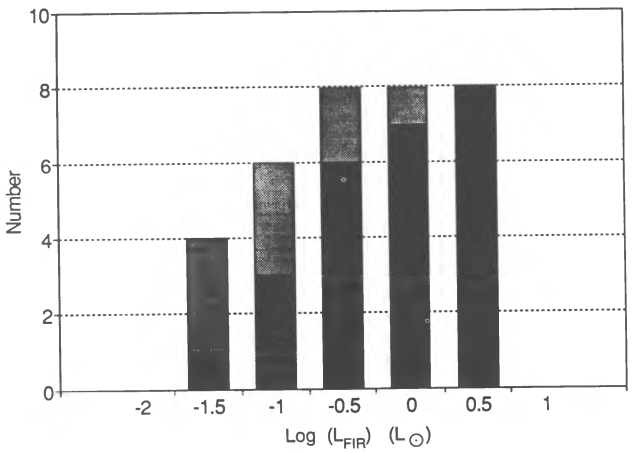

FIG. 5.—Luminosity function binned in half-decade intervals for sources with optical ID classes 4–7, corresponding to Class I objects in the nomenclature of Adams et al. (1987). The luminosity used is L_{FIR} from Table 5. Corrections to this luminosity for emission shortward of 7 μm should not exceed 10%–20%. Objects with light shading indicate sources with $I_{\nu}(100\ \mu\text{m}) < 15$ MJy sr^{-1} which may be galaxies rather than embedded sources within Taurus. As described in the text, the plot includes the four sources missed in this sample, but found by other authors.

factor of 3 deeper than KHSS. As discussed above, the completeness of the sample at this level is estimated to be about 80%–90%. Lightly shaded areas of the distribution shown objects with $I_\nu(100\ \mu\text{m}) \leq 15$ MJy sr^{-1} which may be galaxies. This contamination appears to become progressively more numerous at faint flux densities. Even without correction for possible contamination by galaxies, the luminosity function drops between 0.1 and 0.3 $L_\odot$, implying that there is a minimum luminosity for young stars in this stage of evolution. When the galaxy correction is included, the drop below 0.3 $L_\odot$ is marked. Due to the effects of incompleteness, no statement can be made about the luminosity function below 0.1 $L_\odot$.

KHSS argue that if present theories of protostellar accretion are correct, then Taurus should have either a large number of low-luminosity embedded sources with $L \sim 1\ L_\odot$, or a smaller number of objects with $L \sim 10\ L_\odot$, depending on whether the accretion time is 10^6 or 10^5 yr, respectively. Our luminosity function (Fig. 5) confirms and extends to lower luminosity the conundrum that the Taurus luminosity function is too flat and has too few high luminosity objects to be explained by straightforward application of accretion theory.

A simple way to express the problem is to note that the existence of sources with luminosities as low as 0.05–0.1 $L_\odot$ argues against a high mass infall rate since rapidly accreting objects could have such low luminosities for only a short period of time. An age estimate for an object deriving its luminosity solely by accretion is given by

$$t \sim \frac{LR}{G\dot{M}^2} = 3.2 \times 10^4 \frac{L_\odot R_\odot}{\dot{M}_6^2}\ \text{yr}\ , \qquad (1)$$

where L is the luminosity and R is the radius of the central star, $\dot{M}$ is the mass accretion rate, and G is the gravitational constant. In the right-hand side of the equation, L and R are in solar units and $\dot{M}$ is in units of $10^{-6}\ M_\odot\ \text{yr}^{-1}$. A representative size for the nascent star is 2 $R_\odot$ (Stahler 1988). A simple estimate of the mass infall rate is given by the collapse of a Jeans mass in a free-fall time (Shu 1977),

$$\dot{M} \sim V^3/G \sim 2.4 \times 10^{-4} V^3\ M_\odot\ \text{yr}^{-1}\ , \qquad (2)$$

where V is the internal velocity of the cloud in km s^{-1}. For typical Taurus line widths of 0.2–0.3 km s^{-1} (Myers & Benson 1983; Benson & Myers 1989), the derived infall rates are of order $\sim 4 \times 10^{-6}\ M_\odot\ \text{yr}^{-1}$. The age of a 0.1 $L_\odot$ object would be only 360 yr! Since it is unlikely that a correlated burst of star formation is taking place across tens of parsecs in Taurus, some aspect of the calculation of the accretion luminosity must be in error.

Decreasing $\dot{M}$ *onto the central star* by roughly a factor of 10 would put the ages of the low luminosity sources into a more acceptable range of 10^4 to 10^5 yr. The difference between the $\dot{M}$ implied by V^3/G and the $\dot{M}$ implied by the ages of the embedded sources could represent the material accumulated in a circumstellar disk ~ 100 AU across; accretion of material into a disk of that size would release negligible luminosity. If a disk provides the major reservoir for the infalling material, then the disk would feed the central star at lower rate consistent with the observed luminosity function, but for a time longer than the 10^5 yr duration of the embedded phase (Myers et al. 1987). If disk material were accreted at a rate of $10^{-6}\ M_\odot\ \text{yr}^{-1}$ for the 10^5 yr embedded phase, then a 0.1 $M_\odot$ disk would provide a steady source of luminosity for T Tauri stars over 10^6 yr with infall onto the central star occurring steadily at a rate of a few $10^{-7}\ M_\odot\ \text{yr}^{-1}$. The luminosity function of embedded sources presented herein and in KHSS, as well as the discoveries of massive disks around T Tauri stars with millimeter and submillimeter observations (Beckwith et al. 1990), and of significant accretion luminosity from one-third of the known T Tauri stars (Rucinski 1985; Strom et al. 1989; Cabrit et al. 1990; Cohen et al. 1989) all provide support for the idea of a two stage infall process: relatively rapid accretion into a disk reservoir, followed by a slower infall onto the central star.

3.2. *Nature of the Single Band Sources*

3.2.1. 12 μm *Only Sources*

The 12 μm only sources were compared with the GSC in an attempt to find faint counterparts. As expected on the basis of an earlier study of high-latitude sources (Beichman et al. 1990) most of the 12 μm only sources have stellar counterparts between 9 and 15 mag. Of the 369 12 μm only objects in the sample, 347 have a GSC counterpart within a 60″ by 15″ error box. Histograms of $V - [12]$ color are shown in Figure 6. It is evident that in Auriga there is a fairly uniform distribution of stars with $4 \leq V - [12] \leq 8$ mag. Many of these objects will be mass-loss stars too faint to have been detected at 25 μm. Taurus shows an additional population of objects with $V - [12] \sim 5$ mag that cannot be explained by simply attenuating the visible light of a population of mass-loss stars.

Skrutskie et al. (1989) observed 16 T Tauri stars at 10 μm with 5 mJy sensitivity using the IRTF and found evidence for disks in half of the stars younger than 3 Myr. While the sensitivity of their observations was about 4 times greater than the FSS, the FSS sample can be used to search for disks across the entire Taurus region. Additional follow-up observations including optical spectroscopy and proper motion studies will be required to determine which sources are young objects within Taurus, possibly T Tauri stars identified for the first time by their dust emission. A full sample of disks around T Tauri stars will help define the lifetime of disks.

3.2.2. 60 μm *Only Sources*

What is the nature of the sources detected only at 60 μm? Galaxies, cirrus, or embedded objects? The differential source counts (Fig. 7) suggest an excess of bright 60 μm sources in Taurus relative to the background of infrared luminous galaxies. The number of objects brighter than 0.5 Jy at 60 μm

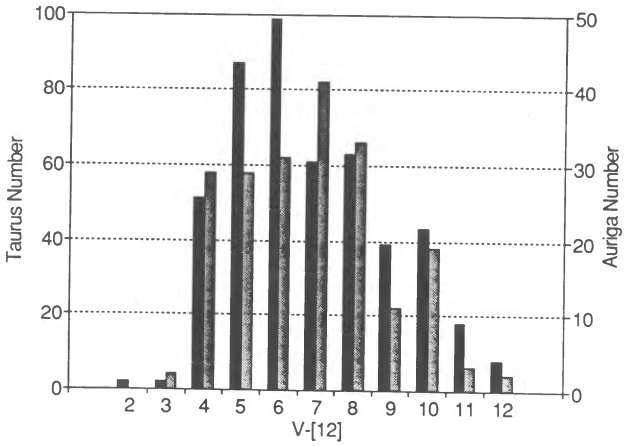

FIG. 6.—Histogram of $V - [12]$ color for Taurus (*dark shading*) and Auriga (*light shading*) regions shows an excess in Taurus of objects with $V - [12] \sim 5$ mag that cannot be accounted for by the effects of extinction.

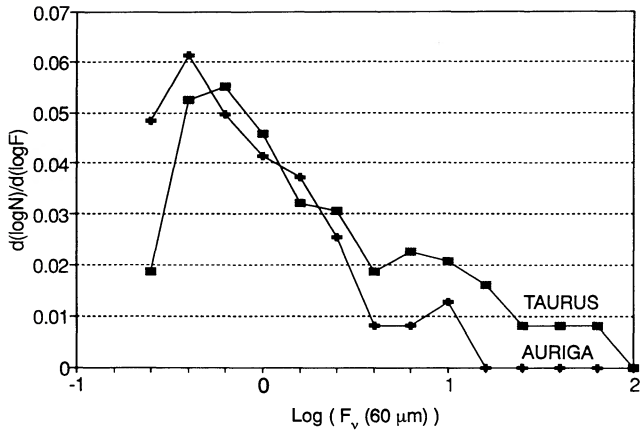

FIG. 7.—Differential number counts in Taurus and Aufiga are plotted as number (deg^{-2}) per logarithmic interval in $f_\nu(60\ \mu m)$ vs. log $[f_\nu(60\ \mu m)]$ for sources detected at 60 μm and without a stellar counterpart as determined from FSS associations.

(with no constraint on detections at other *IRAS* wavelengths) and without a stellar counterpart is 106 in Auriga and 151 in Taurus, corresponding to surface densities of 0.57 ± 0.06 (deg^{-2}) and 0.81 ± 0.06 (deg^{-2}); the uncertainties are estimated from Poisson statistics. At this flux density level, one expects approximately 0.4 galaxy (deg^{-2}) (Soifer, Houck, & Neugebauer 1987). Thus, while there is at most only a slight excess of 60 μm sources in Auriga, possibly due to unaccounted-for stars or cirrus detections, there is a clear excess of 60 μm sources in Taurus relative to Auriga and to that expected from galaxies.

To explain the fact that the number of 60 μm only objects in Auriga is greater than the number in Taurus (Table 2), note that 60 μm source counts (Fig. 7) extend about a factor of 1.6 deeper in Auriga than in Taurus, presumably due to a lower level of cirrus confusion. Since the integrated 60 μm source counts in Auriga follow closely the $f_\nu^{-3/2}$ law expected for galaxies, a factor of $\sim 1.6^{3/2} = 2.0$ more 60 μm galaxies are expected in Auriga than in Taurus.

Many of the Taurus objects in Table 7 could be galaxies. The amount of interstellar material, measured by $I_\nu(100\ \mu m)$, can be used to reject galaxies, since 60 μm sources associated with small amounts of interstellar material are more likely to be galaxies than those found toward molecular clouds. Seven of the 28 unresolved objects in Table 7 have $I_\nu(100\ \mu m) \geq 10$ MJy sr^{-1}, corresponding to $A_V \geq 2.5$ mag; all but one of these sources is found in an optically blank field. These characteristics strongly suggest the presence of a condensed object within a significant amount of interstellar gas. The group of 60 μm only sources with low $I_\nu(100\ \mu m)$ is probably heavily contaminated by galaxies.

The sources with $I_\nu(100\ \mu m) \geq 10$ MJy sr^{-1} have an average luminosity of 0.028 $L_\odot$ and are the best candidates yet identified for stars in the earliest stages of formation. The age problem discussed for the multiband embedded objects applies even more forcefully for the 60 μm only objects. The average age of a 0.03 $L_\odot$ object accreting at $4 \times 10^{-6}\ M_\odot$ yr^{-1} is only 120 yr. If any of these sources are self-luminous, the mass infall rate on to the star must be considerably smaller than inferred from the average linewidths in Taurus. Observations including optical or millimeter spectroscopy, and high spatial-resolution mapping at either far infrared or at millimeter wavelengths are needed to clarify the nature of these objects.

4. CONCLUSIONS

The *IRAS* Faint Source Survey has been used to generate a sample of suspected young stellar objects over an area covering 187 deg^2. Sixty-three multiband sources, selected on the basis of their colors and lack of stellar counterparts, form a sample thought to be 80% to 90% complete down to a luminosity limit of 0.1 $L_\odot$. This sample can be used for complete, luminosity-limited studies of multiplicity, circumstellar disk formation, outflow physics, and other investigations relating to the physics of star formation. Future papers in this series will describe near-infrared imaging and millimeter observations of the samples presented in this paper.

Two samples of single-band sources, 12 μm and 60 μm only, have been generated as well. Most of the 12 μm only objects have faint stellar counterparts in the Guide Star Catalog and are probably stars with small amounts of mass loss (Beichman et al. 1990). A sample of 60 μm only objects unresolved by *IRAS* may represent the youngest protostars yet observed.

The large number of objects with low luminosities, $\sim 0.1\ L_\odot$, is difficult to understand within the confines of a model invoking mass infall directly onto a central young star. The infall of material into a massive, $\sim 0.1\ M_\odot$, protostellar nebula that forms a reservoir for the more gradual build-up of a star over 10^5 yr provides a reasonable scenario that fits with other observations of embedded sources and T Tauri stars.

The work described here was supported in part by a grant from NASA's Astrophysics Data Analysis Program. C. A. B. gratefully acknowledges the hospitality of the Institute for Advanced Study and receipt of travel support from the Ecole Normale Supérieure. The authors thank the referee, S. Kenyon, for useful comments and for identifying some of the sources as galaxies or T Tauri stars based on unpublished data. The research described in this paper was carried out, in part, by the Jet Propulsion Laboratory, California Institute of Technology, under a contract with the National Aeronautics and Space Administration.

REFERENCES

Adams, F., Lada, C., & Shu, F. 1987, ApJ, 312, 788
Beckwith, S., Sargent, A. I., Chini, R. S., & Güsten, R. 1990, AJ, 99, 924
Beichman, C. A. 1990, in From Ground-Based to Space-Borne Submillimeter Astronomy, ed. J. P. Swings, D. Fraipont, & B. Koldreich (ESA SP-314), 179
Beichman, C. A., Chester, T., Gillett, F. C., Low, F. J., Matthews, K. W., & Neugebauer, G. 1990, AJ, 99, 1569
Beichman, C. A., Myers, P. C., Harris-Law, S., Mathieu, R., Benson, P. J., & Jennings, R. E. 1986, ApJ, 307, 337
Benson, P. J., & Myers, P. 1989, ApJS, 71, 89
Boulanger, F., & Pérault, M. 1988, ApJ, 330, 964
Burstein, D., & Heiles, C. 1977, AJ, 87, 1165
Cabrit, S., Edwards, S., Strom, S. E., & Strom, K. M. 1990, ApJ, 354, 687
Cernicharo, J., & Guélin, M. 1987, A&A, 176, 299
Cohen, M., Emerson, J. P., & Beichman, C. A. 1989, ApJ, 339, 455
Elias, J. 1978, ApJ, 224, 857
Emerson, J. P. 1989, in Formation and Evolution of Low Mass Stars, ed. A. K. Dupree & M. T. V. T. Lago (Dordrecht: Kluwer), 193
Harris-Law, S., Clegg, P. E., & Hughes, J. 1988, MNRAS, 235, 441
Helou, G. 1986, ApJ, 311, L33
Herbig, G. H. 1977, ApJ, 214, 747
Herbig, G. H., & Bell, K. R. 1988, Lick Obs. Bull. IIII
IRAS Catalogs and Atlases, Explanatory Supplement 1988, ed. C. A. Beichman, G. Neugebauer, H. J. Habing, P. E. Clegg, & T. J. Chester (Washington, DC: GPO)

IRAS Point Source Catalog, Version 2, 1988, Joint *IRAS* Science Working Group (Washington, DC: GPO)
Jenkner, H., Lasker, B. M., Sturch, C. R., McLean, B. J., Shara, M. M., & Russell, J. L. 1990, AJ, 99, 2081
Kenyon, S. J., Hartmann, L. W., Strom, K. M., & Strom, S. E. 1990, AJ, 99, 869 (KHSS)
Kleinmann, S. E., Cutri, R. M., Young, E. T., Low, F. J., & Gillett, F. C. 1986, Explanatory Supplement to the *IRAS* Serendipitous Survey Catalog, IPAC preprint
Ladd, E. F., et al. 1991, ApJ, 366, 203
Langer, W. D., Wilson, R. W., Goldsmith, P. F., & Beichman, C. A. 1989, ApJ, 337, 355
Lasker, B. M., Sturch, C. R., McLean, B. J., Russell, J. L., Jenkner, H., & Shara, M. M. 1990, AJ, 99, 2019
Low, F. J., et al. 1984, ApJ, 248, L19
Moshir, M., et al. 1989, Explanatory Supplement to the *IRAS* Faint Source Survey, IPAC preprint 44
Myers, P., & Benson, P. J. 1983, ApJ, 266, 309
Myers, P., Fuller, G. A., Mathieu, R. D., Beichman, C. A., Benson, P. J., Schild, R. E., & Emerson, S. P. 1987, ApJ, 319, 340
Rucinski, S. M. 1985, AJ, 90, 2321
Sargent, A. 1979, ApJ, 233, 163
Scalo, J. 1990, in Physical Processes in Fragmentation and Star Formation, ed. R. Capuzzo-Delcetta et al. (Dordrecht: Kluwer), 151
Schloerb, F. P., & Snell, R. L. 1984, ApJ, 283, 129
Shu, F. 1977, ApJ, 214, 488
Shu, F., Adams, F. C., & Lizano, S. 1987, ARA&A, 25, 23
Skrutskie, M. F., Dutkevitch, D., Strom, S. E., Edwards, S., & Strom, K. M. 1989, AJ, 99, 1187
Snell, R. L., Heyer, M. H., & Schloerb, F. P. 1989, ApJ, 337, 739
Soifer, B. T., Houck, J. R., & Neugebauer, G. 1987, ARA&A, 25, 187
Stahler, S. W. 1988, ApJ, 332, 804
Strom, K. M., Strom, S. E., Edwards, S., Cabrit, S., & Skrutskie, M. F. 1989, AJ, 97, 1451
Terebey, S., Beichman, C. A., Gautier, T. N., & Hester, J. J. 1990, ApJ, 362, L63
Ungerechts, H., & Thaddeus, P. 1987, ApJS, 63, 645
Zuckerman, B., & Dyck, H. M. 1986, ApJ, 304, 394